Spin-orbit-coupled atomic Fermi gases in two-dimensional optical lattices in the presence of a Zeeman field

Zlatko Koinov* and Shanna Pahl
Department of Physics and Astronomy, University of Texas at San Antonio, San Antonio, Texas 78249, USA
(Received 27 December 2016; published 30 March 2017)

We investigate the single-particle and collective excitations of a Rashba spin-orbit-coupled atomic Fermi gas with attractive interaction, loaded in a two-dimensional (2D) square optical lattice, in the presence of an effective out-of-plane Zeeman field. Our numerical calculations show that the many-body physics of the Bardeen-Cooper-Schrieffer (BCS) side is strongly modified compared to the Fermi gases in the free space. The physics behind this statement lies in the fact that in the 2D lattice case the single-particle ground-state energy is four times degenerated, while without a lattice structure the ground state is infinitely degenerate, and because of that, the spin-orbit coupling (SOC) in optical lattices gives rise to unusual properties entirely different from the continuum. For example, in the continuum, the pairing gap as well as the condensate fraction is strongly enhanced by the SOC strength on the BCS side. In the presence of lattice geometry the gap and the condensate fraction increase as a function of the SOC strength only at small fillings and a weak attraction limit. Moreover, we found that the speed of sound also exhibits different behavior: in the 3D and 2D continua, the slope of the Goldstone mode decreases as a function of the SOC strength, while in the lattice case the speed of sound increases monotonically with the SOC strength.

DOI: 10.1103/PhysRevA.95.033634

I. INTRODUCTION

The experimental realization of spin-orbit coupling (SOC) in ultracold atoms [1–3] has initiated substantial theoretical efforts to study its effects in two-dimensional (2D) and three-dimensional (3D) Fermi gases [4–22]. This is because spin-orbit (SO)-coupled systems with a Zeeman field, which breaks the population balance, can lead to novel types of exotic superfluid phases that may support Majorana fermions [23,24].

Although Rashba SO-coupled atomic Fermi gases in free space have been extensively investigated, the entirely different case of an attractive Fermi gas in a square optical lattice with SOC has been mostly studied in the presence of an external non-Abelian gauge field [25–40]. In what follows, we study a population-balanced mixture of fermion atoms with an s-wave pairing interaction loaded in a square 2D optical lattice, with Rashba SOC and an external out-of-plane Zeeman field. We use a small Zeeman field, because in this regime the pairing between atoms on the same Fermi surface is preferred; this is the normal Bardeen-Cooper-Schrieffer (BCS) superfluid (for a larger Zeeman field, the topological BCS superfluid as well as the Fulde-Ferrell-Larkin-Ovchinnikov superfluid phases appears) [36,37].

A. SO-coupled atoms in continuous space

It is widely assumed that the two-body problem is the key to understanding the physics of SO-coupled Fermi gases. Consider, for example, the two-body problem in the case of a 3D spin-1/2 Fermi gas with Rashba SOC and an external out-of-plane Zeeman field. The spectrum of the single-particle excitations is $\epsilon_{\pm}(\mathbf{k}) = \varepsilon(\mathbf{k}) \pm \sqrt{h^2 + \lambda^2 k_{\perp}^2}$, where $\varepsilon(\mathbf{k}) = \hbar^2\mathbf{k}^2/(2m) - \mu$, μ is the chemical potential, h is the strength of the Zeeman field, and λ is the SOC constant. A bound state exists if its energy $E_B < 0$ is less than twice the minimum of the single-particle ground-state energy $\epsilon_{\min}$, i.e., $E_B - 2\epsilon_{\min} = \varepsilon_b < 0$. If the value of the Zeeman field exceeds the threshold value $h > h_c = m\lambda^2/\hbar^2$, a unique lowest single-particle state $\epsilon_{\min} = -h$ occurs at $\mathbf{k} = 0$, and the bound state exists only on the BEC side of the Feshbach resonance. If $h < h_c$, the minimum single-particle energy

$$\epsilon_{\min} = -[m\lambda^2/(2\hbar^2) + \hbar^2 h^2/(2m\lambda^2)]$$

occurs continuously along a ring of radius $k_{\perp} = \sqrt{m^2\lambda^2/\hbar^2 - \hbar^2/\lambda^2}$ in the (k_x,k_y) plane [7]. This reduces the effective dimensionality. Since the single-particle ground state is not unique, the ground state of a boson condensate is also not unique, and because the density of states is a constant at low energies, a two-body bound state appears for any weak attractions, and therefore, the bound state exists even on the BCS side. The corresponding two-body bound-state energy E_B can be obtained by numerically solving the two-body bound-state equation. In the Gaussian approximation, E_B at zero temperature is determined by the following equation [7,10,11,15,18]:

$$\frac{1}{U} = -\frac{1}{2N}\sum_{\mathbf{k}}\left[\frac{1}{E_B - 2\epsilon_+(\mathbf{k})} + \frac{1}{E_B - 2\epsilon_-(\mathbf{k})}\right] + \frac{1}{N}\sum_{\mathbf{k}}\left[\frac{4h^2}{[E_B - 2\varepsilon(\mathbf{k})][E_B - 2\epsilon_+(\mathbf{k})][E_B - 2\epsilon_-(\mathbf{k})]}\right]. \quad (1)$$

Here, the interaction strength U needs to be regularized in a standard manner by means of the s-wave scattering length a_s. According to the solutions of Eq. (1), an increase in the SOC strength λ leads to a deeper bound state; i.e., the binding energy strongly depends on the SOC strength. Since these

*Zlatko.Koinov@utsa.edu

bound states are caused by the SOC, they have been referred to as rashbons [7,10,11,15,18].

In the many-particle problem, the single-particle spectrum is $E_{\pm}(\mathbf{k}) = \{\lambda^2 k_\perp^2 + \Delta^2 + h^2 + \varepsilon^2(\mathbf{k}) \pm 2\sqrt{h^2\Delta^2 + \varepsilon^2(\mathbf{k})[h^2 + \lambda^2 k_\perp^2]}\}^{1/2}$, where the chemical potential μ and the pairing gap Δ can be obtained by numerically solving the corresponding number and gap equations. It was determined, in Ref. [10], that in the large-SOC limit the chemical potential $|\mu| = |E_B|/2 - \mu_b$ becomes negative since μ_b, the chemical potential for composite bosons (which is positive due to the repulsion between rashbons), decreases with increasing λ, as shown in the inset in Fig. 4.

The convergence of the chemical potential and one-half of the bound-state energy on the BCS side, evident in the two-body problem, suggests that Rashba SOC may trigger a new type of crossover to rashbon BEC in the many-body problem of fermions. Thus, the BCS-BEC crossover is of special interest, and it has been stated that the contributions of the singlet and triplet pairings to the condensate fraction, separately, characterize the crossover better than other quantities [8].

B. Square optical lattice with an external non-Abelian gauge field

Here we study the system of a two-component Fermi gas moving in an optical square lattice with an external non-Abelian gauge field that can be described by a single-band negative-U Hubbard model [30,32,40]. Let us assume that the spin-conserved hopping term is proportional to $t\cos(\lambda)$, and the spin-flipped term is in proportion to $t\sin(\lambda)$ (energy units are in terms of the tunneling strength $t = 1$, and spatial units are in terms of lattice constant $a = 1$). The lowest single-particle state $\epsilon_{\min} = -2\sqrt{3 + \cos(2\lambda)}$ is four times degenerate and occurs at four points in momentum space:

$$\pm k_x, \pm k_y = \cos^{-1}\left(\frac{\cos(\lambda)}{\sqrt{\cos^2(\lambda) + \sin^2(\lambda)/2}}\right).$$

As pointed out in Ref. [32], the interplay between interactions and the Dirac spectrum generated by Rashba coupling leads to interesting behavior with respect to the filling factor, especially in the weak- and intermediate-attraction regimes. It was found that for small fillings, not only does the chemical potential increase with the SOC (as opposed to the continuous system), but also the pairing gap and condensate fraction are enhanced by the SOC. However, for close to half-filling, they are suppressed.

To illustrate this, in Fig. 1(a) we show the chemical potential, gap, and $\epsilon_{\min}$, and in Fig. 1(b) the total condensate fraction, all calculated by numerically solving the corresponding number and gap equation in the mean-field approximation for filling $f = 0.1$ and weak interaction strength $U = 2t$. As shown, above the critical SOC $\lambda_c = 0.4\pi/2$, the chemical potential approaches $\epsilon_{\min}$, and both the gap and the total condensate fraction increase rapidly. This is a fingerprint for the formation of SOC-induced bound states. Furthermore, the authors of Ref. [32] show that λ_c increases when the filling is increased, but after $f = 0.7$, the condensate fraction begins to decrease.

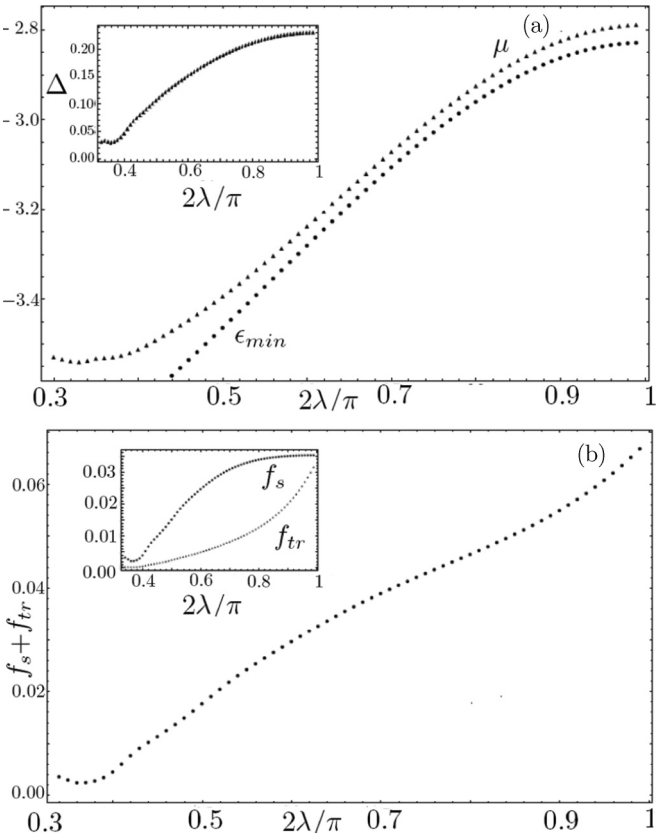

FIG. 1. (a) Chemical potential μ, pairing gap Δ, the minimum of the single-particle ground state energy $\epsilon_{\min}$ versus λ, and (b) the total condensate fraction $f_c = f_s + f_{\rm tr}$ versus λ (f_s and $f_{\rm tr}$ are the singlet and triplet contributions) of a Fermi gas in a square optical lattice subject to a Rashba non-Abelian SOC of strength λ. The on-site attractive strength is $U = 2t$, and the filling factor is $f = 0.1$.

In what follows, we present our study of the interplay between the SOC, the strength of the interaction, and the Zeeman field in lattice systems and compare our findings with those for the aforementioned non-Abelian lattice system [32,40] and free-space systems (our results can be compared only to the results obtained in Ref. [40] which correspond to the case where the next-nearest-neighbor hopping is set to 0).

The paper is organized as follows. In Sec. II, we use the mean-field single-particle Green's function to obtain the singlet and triplet pairing amplitudes and the singlet and triplet condensate fractions. In Sec III, we use the functional-integral formalism to obtain the Bethe-Salpeter (BS) equation in the generalized random phase approximation (GRPA) for the spectrum of the two-particle excitations. In the GRPA, single-particle excitations are replaced with those obtained in the mean-field (MF) approximation; the collective modes are obtained by solving the BS equation, in which the single-particle Green's functions are calculated in the mean-field approximation, and the BS kernel is a sum of the direct and exchange interactions. In diagrammatic language, the kernel is represented by ladder and bubble diagrams. We compare the speed of sound, obtained by the BS formalism, to the corresponding speed obtained in the Gaussian approximation. Since the Gaussian approximation does not take into account

the exchange interaction [41] (represented by the bubble diagrams), the speed of sound is overestimated by about 10%–20% compared to the value provided by the BS equation. We also show that in the two-body problem ($\Delta = 0$), the BS formalism provides the same bound-state-energy equation, (1), as in the Gaussian approximation. We summarize in Sec. IV.

II. SINGLE-PARTICLE GREEN's FUNCTION OF THE RASHBA SOC AND ZEEMAN FIELD IN A SQUARE OPTICAL LATTICE IN THE MEAN-FIELD APPROXIMATION

We restrict the discussion to the case of atoms confined to the lowest-energy band (single-band model), with two possible states described by pseudospins $\sigma = \uparrow, \downarrow$. There are M atoms distributed along N sites, and the corresponding filling factor $f = M/N$ is smaller than unity. The Hamiltonian for a uniform system is $\hat{H} = \hat{H}_0 + \hat{H}_{\rm SOC} + \hat{H}_Z$, where the Hubbard Hamiltonian is

$$\widehat{H}_0 = -t \sum_{\langle i,j\rangle,\sigma} \psi^\dagger_{i,\sigma}\psi_{j,\sigma} - U\sum_i \widehat{n}_{i,\uparrow}\widehat{n}_{i,\downarrow} - \mu \sum_{i,\sigma} \widehat{n}_{i,\sigma}. \quad (2)$$

Here $t = 1$ is the tunneling strength of the atoms between nearest-neighbor sites, μ is the chemical potential, and $\widehat{n}_{i,\sigma} = \psi^\dagger_{i,\sigma}\psi_{i,\sigma}$ is the density operator at site i. The Fermi operator $\psi^\dagger_{i,\sigma}$ ($\psi_{i,\sigma}$) creates (destroys) a fermion at lattice site i with pseudospin projection σ. The symbol $\sum_{\langle ij\rangle}$ means the sum over nearest-neighbor sites on the 2D lattice. The strength of the on-site interaction is $U > 0$, which corresponds to attractive interaction. The SOC part of the Hamiltonian is given by

$$\widehat{H}_{\rm SOC} = -\imath\lambda \sum_{\langle i,j\rangle} (\psi^\dagger_{i,\uparrow},\ \psi^\dagger_{j,\downarrow})(\vec{\sigma}\times \mathbf{d}_{i,j})_z \begin{pmatrix}\psi_{i,\uparrow}\\ \psi_{j,\downarrow}\end{pmatrix}, \quad (3)$$

where λ is the Rashba SOC coefficient, $\vec{\sigma} = (\sigma_x,\sigma_y,\sigma_z)$, the components $\sigma_{x,y,z}$ are the Pauli matrices, and $\mathbf{d}_{i,j}$ is a unit vector along the line that connects site j to site i. The out-of-plane Zeeman field is described by the term $\widehat{H}_Z$:

$$\widehat{H}_Z = h\sum_i (\psi^\dagger_{i,\uparrow},\ \psi^\dagger_{i,\downarrow})\sigma_z \begin{pmatrix}\psi_{i,\uparrow}\\ \psi_{i,\downarrow}\end{pmatrix}. \quad (4)$$

The spectrum of the single-particle excitations in the two-body problem is $\epsilon_\pm(\mathbf{k}) = \varepsilon(\mathbf{k}) \pm \sqrt{h^2 + 4\lambda^2[\sin^2(k_x) + \sin^2(k_y)]}$, where $\varepsilon(\mathbf{k}) = 2[1 - \cos(k_x)] + 2[1 - \cos(k_y)]$ is the tight-binding energy in a 2D optical lattice.

In the case where $h > h_c = 2\lambda^2/t$, the lowest single-particle state $\epsilon_{\rm min} = -h$ is centered at $\mathbf{k} = 0$. If $h < h_c$, the lowest single-particle state is four times degenerate and occurs at four points in momentum space:

$$\pm k_x a, \pm k_y a = \cos^{-1}\left(\frac{t\sqrt{h^2 + 8\lambda^2}}{\lambda\sqrt{8t^2 + 4\lambda^2}}\right).$$

The corresponding minimum is

$$\epsilon_{\rm min} = 4t - \sqrt{\frac{(h^2 + 8\lambda^2)(2t^2 + \lambda^2)}{\lambda^2}}, \quad h < h_c.$$

The two-particle bound energy $E_B < 0$ (in units t) in a 2D optical lattice satisfies the conditions

$$\frac{|E_B|}{2} > h, \quad h > h_c,$$
$$\frac{|E_B|}{2} > 4\sqrt{1 + \frac{\lambda^2}{2} + \frac{h^2}{16}\left(1 + \frac{2}{\lambda^2}\right)} - 4, \quad h < h_c. \quad (5)$$

When $h < h_c$ and $\lambda \gg 1$, we have $|\epsilon_{\rm min}| \propto \lambda$.

By definition, the single-particle Green's function $\hat{G}(x_1; y_2)$ is a 4×4 matrix whose elements are $G_{\sigma,\sigma'}(x_1; y_2) = -\langle \widehat{T}_u(\psi_\sigma(x_1)\psi^\dagger_{\sigma'}(y_2))\rangle$, where the symbol $\langle \dots \rangle$ means that the thermodynamic average is taken. Here, we have introduced composite variables, $y_2 = \{\mathbf{r}_2, u_2\}$ and $x_1 = \{\mathbf{r}_1, u_1\}$, where $\mathbf{r}_1$ and $\mathbf{r}_2$ are the lattice-site vectors, and according to the imaginary-time (Matsubara) formalism the variables u_1 and u_2 range from 0 to $\hbar\beta = \hbar/(k_B T)$. Throughout this paper we have assumed $\hbar = k_B = 1$.

The single-particle properties are studied within the standard mean-field approximation, such that the chemical potential and the pairing gap are obtained by solving the number and the gap equations self-consistently. The two equations as well as the matrix elements of the mean-field single-particle Green's function are provided in Appendix A. The single-particle excitations are defined by the four poles $\pm\omega_1(\mathbf{k})$ and $\pm\omega_2(\mathbf{k})$ of the Green's function. It is worth mentioning that Monte Carlo simulations have shown that, at zero temperature, beyond-mean-field effects are negligible on the BCS side [42,43].

Next, we show various mean-field quantities of physical interest, such as the chemical potential, the pairing gap, the singlet and triplet pairing amplitudes, and the singlet and triplet condensate fractions. We focus on the zero-temperature case, assuming a filling factor of $f = 0.5$ and a Zeeman field $h = 0.4t$. We show in Fig. 2(a) the chemical potential μ and in Fig. 2(b) the gap Δ, as functions of the strength of the attractive interaction U, for different values of the Rashba SOC strength, and compare them to the case of a 2D free Fermi gas [8] and a non-Abelian system [32,40].

As in the case of a 2D free Fermi gas, the chemical potential is pushed toward more negative values when the SOC increases, and it becomes negative on the BCS side when the strength of the SOC is increased above $\lambda_0 \approx 2t$. In the free case, as well as our lattice case and the non-Abelian case, μ decreases with increasing SOC strength. However, there is little dependence of μ on the interaction strength for this filling factor, $f = 0.5$ [32].

The gap differs more significantly from that in the free case. At a fixed interaction, the gap is increased for higher SOC in the free case and suppressed for higher SOC in both lattice cases. Furthermore, as the interaction goes from BCS to BEC in the free case, the gaps for the range of SOC strengths increase significantly and converge. For our lattice case, the gap decreases for the range of SOC strengths, which converge as the interaction strength decreases to 0. However, our results for the gap seem to have a progression consistent with the non-Abelian system [32,40].

In Fig. 3, we plot the chemical potential and the gap as functions of the Rashba SOC strength in the weak-coupling limit when $U = 5t$. Contrary to the free Fermi gas [8,9,19]

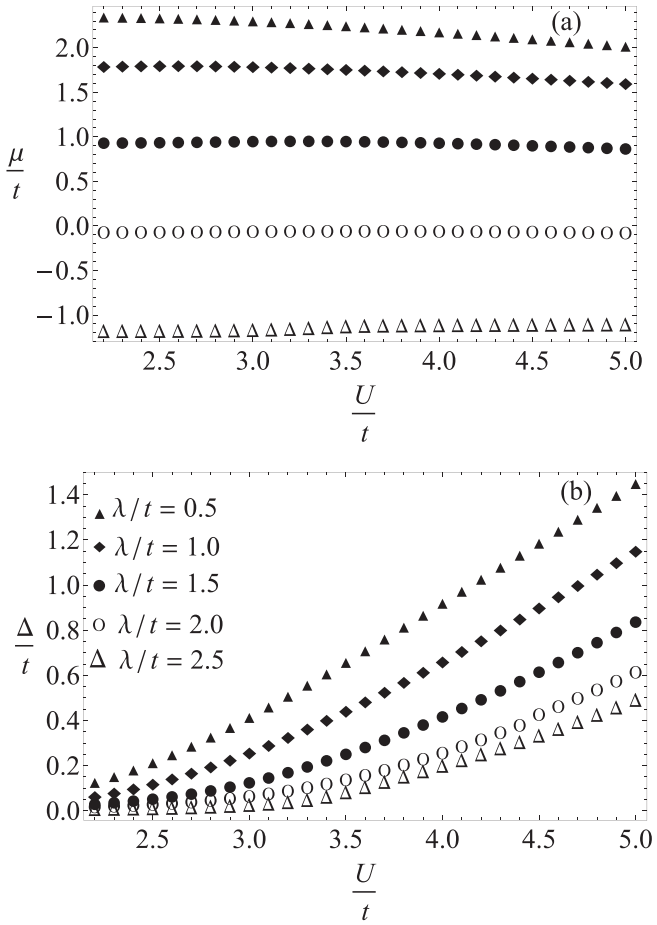

FIG. 2. Zero-temperature mean-field (a) chemical potential μ and (b) gap Δ for fermion atoms in a 2D optical lattice as a function of the strength of the attractive interaction U for different values of the Rashba SOC strengths λ at a Zeeman field $h = 0.4t$ and $f = 0.5$.

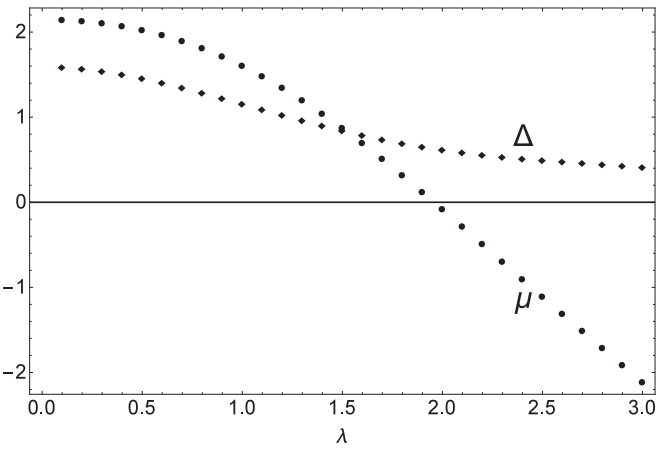

FIG. 3. Zero-temperature gap Δ and chemical potential μ as a function of the Rashba SOC strength λ for Fermion atoms in a 2D optical lattice. System parameters are $U = 5t$, $f = 0.5$, and $h = 0.4t$ (λ, Δ, and μ are in units of t).

the gap decreases when the SOC increases, and the chemical potential does not approach $2\epsilon_{\min}$ even in the limit of very strong SOC (see Fig. 4). We also calculated the chemical potentials for interaction strengths $U = 3t$ and $4t$ as functions of λ, but their differences from $5t$ values were statistically insignificant—μ still diverges from $\epsilon_{\min}$—thus they are not presented in Fig. 4.

From the mean-field elements of the single-particle Green's function, one can obtain the momentum distribution for the two spin components $n_\uparrow(\mathbf{k}) = \langle \psi^\dagger_{\mathbf{k}\uparrow}\psi_{\mathbf{k}\uparrow}\rangle$ and $n_\downarrow(\mathbf{k}) = \langle \psi^\dagger_{\mathbf{k}\downarrow}\psi_{\mathbf{k}\downarrow}\rangle$. In Fig. 5, we plot the zero-temperature momentum distributions for the two spin components, for two values of the Zeeman field. Without a Zeeman field, we have equal populations of both spin components. However, for a Zeeman field in the up direction, the spin-up component has a smaller population, consistent with the results for a two-component free Fermi gas with a Zeeman field [7].

Another interesting feature of the SOC is that the pairing field contains both a singlet and a triplet component. The singlet, $\Phi_{\downarrow\uparrow}(\mathbf{k}) = -\Phi_{\uparrow\downarrow}(\mathbf{k}) = \langle \psi_{\mathbf{k}\downarrow}\psi_{-\mathbf{k}\uparrow}\rangle$, and triplet, $\Phi_{\uparrow\uparrow}(\mathbf{k}) = \langle \psi_{\mathbf{k}\uparrow}\psi_{-\mathbf{k}\uparrow}\rangle$ and $\Phi_{\downarrow\downarrow}(\mathbf{k}) = \langle \psi_{\mathbf{k}\downarrow}\psi_{-\mathbf{k}\downarrow}\rangle$, amplitudes, obtained by means of the Green's function elements $G^{\rm MF}_{23}$, $G^{\rm MF}_{13}$, and $G^{\rm MF}_{24}$, are defined in Appendix A. In Fig. 6, we plot the magnitudes of the singlet and triplet pairing amplitudes for different values of the Zeeman field h at zero temperature. As shown, the Zeeman field enhances the triplet pairing and reduces the singlet pairing, consistent with free-gas results with a Zeeman field [7,10].

With the help of the pairing amplitudes, one can calculate the condensate fraction $f_c = f_s + f_{\rm tr}$, where f_s and $f_{\rm tr}$ are the singlet and triplet contributions, respectively. At zero temperature, we have $f_s = \frac{2}{N}\sum_{\mathbf{k}} |\Phi_{\downarrow\uparrow}(\mathbf{k})|^2$ and $f_{\rm tr} = \frac{1}{N}\sum_{\mathbf{k}} (|\Phi_{\uparrow\uparrow}(\mathbf{k})|^2 + |\Phi_{\downarrow\downarrow}(\mathbf{k})|^2)$. We show in Fig. 7 the zero-temperature singlet f_s and triplet $f_{\rm tr}$ condensate fractions as functions of the strength of the attractive interaction U, for different values of the Rashba SOC strength. In our case and in the non-Abelian case, the progression of the singlet

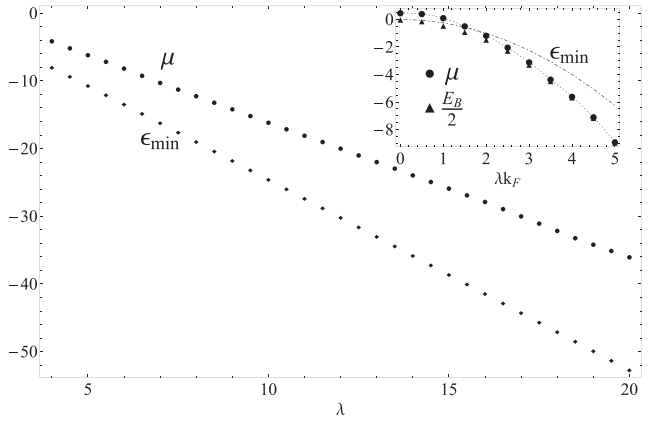

FIG. 4. The chemical potential μ and the single-particle ground-state energy $\epsilon_{\min}$ as functions of the Rashba SOC strength for fermion atoms in a 2D optical lattice. System parameters are $U = 5t$, $f = 0.5$, and $h = 0.4t$ (all energies are in units of t). Inset: Convergence of the chemical potential μ and half of the bound-state energy $E_B/2$ as functions of the Rashba SOC strength for a homogeneous unitary Fermi gas at zero temperature in the absence of a Zeeman field. Numerical values of μ and E_B (in units of the Fermi energy $E_F = \hbar^2 k_F^2/2m$) have been calculated in [10].

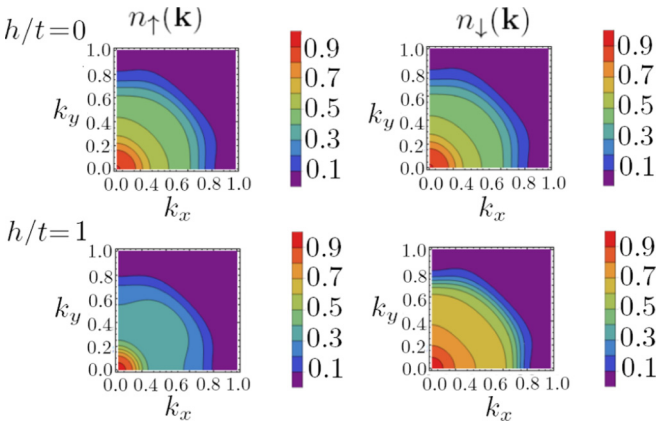

FIG. 5. Zero-temperature momentum distributions for the two spin components for different values of the Zeeman field h at $\lambda = 1t$, $f = 0.5$, and $U = 5t$ (k_x and k_y are in units of π/a). For $h = 0$ we always have equal populations in both spin components, but for $h > 0$ the spin-up component has a smaller population.

condensation curves as the interaction increases is consistent with the behavior of the pairing gap curves. Furthermore, the singlet condensation increases when U increases; but at a fixed U, f_s is suppressed by the SOC.

The singlet f_s, triplet $f_{\rm tr}$, and full f_c condensate fractions versus the SOC, for interaction strength $U = 5t$, are plotted in Fig. 8. For a positive chemical potential, the triplet condensation fraction is less than the singlet one. As the chemical potential decreases and becomes negative ($\lambda \approx 1.96t$), the two fractions converge to each other. We see in the inset that f_c decreases with respect to λ. For $\lambda = 3t$, we have that f_c is about 10% of f. In the weak-interaction regime, for both our case and the 2D free space without a Zeeman field [8], the condensate fraction is small.

Under a different scenario, such that when the Zeeman field is removed, the filling factor is reduced to $f = 0.1$, and the interaction strength is weak, $U = 2.5t$, the gap and the condensate fraction increase dramatically above a critical λ_c (for our case $\lambda \approx 0.7t$), which is similar to the non-Abelian

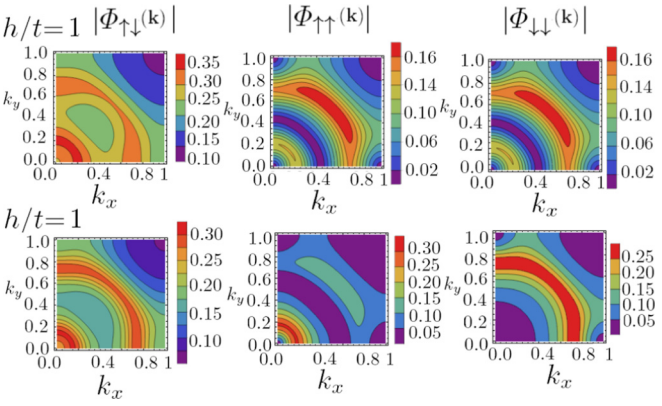

FIG. 6. Magnitudes of the singlet and triplet pairing amplitudes for different values of the Zeeman field h at zero temperature and at $\lambda = 1t$, $f = 0.5$, and $U = 5t$ (k_x and k_y are in units of π/a). The Zeeman field enhances the triplet pairing and reduces singlet pairing.

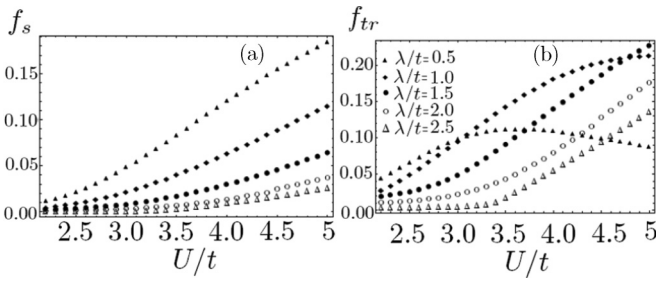

FIG. 7. Zero-temperature (a) singlet and (b) triplet condensate fractions for fermion atoms in a 2D optical lattice as a function of the strength of the attractive interaction U for different values of the Rashba SOC strengths λ at a Zeeman field $h = 0.4t$ and $f = 0.5$.

case (see Fig. 9). Therefore, in accordance with Ref. [32], formation of the SOC-induced bound states takes place.

III. TWO-PARTICLE EXCITATION SPECTRUM IN THE BETHE-SALPETER APPROXIMATION

The results in the previous section were obtained by applying the mean-field decoupling of the quartic term to the interaction part of the Hamiltonian $\widehat{H}_0$. To go beyond the mean-field approximation, we use the idea that one can transform the quartic terms into quadratic form by making the Hubbard-Stratonovich transformation for the fermion operators. In contrast to the previous approaches, where, after performing the Hubbard-Stratonovich transformation the fermion degrees of freedom are integrated out, we decouple the quartic problem by introducing a model system which consists of a multicomponent boson field A_α interacting with fermion fields $\psi^\dagger$ and ψ.

There are three advantages to keeping both the fermion and the boson degrees of freedom. First, the approximation that is used to decouple the self-consistent relation between the fermion self-energy and the two-particle Green's function automatically leads to conserving approximations. This is because it relies on the fact that the BS kernel can be written as

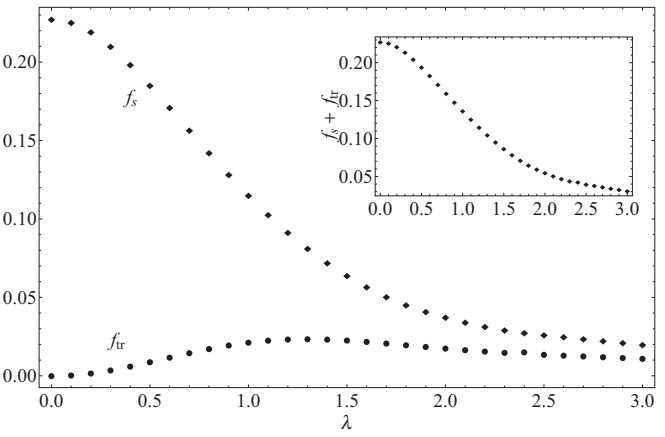

FIG. 8. Zero-temperature singlet f_s, triplet $f_{\rm tr}$, and full $f_c = f_s + f_{\rm tr}$ condensate fractions as a function of the Rashba SOC strength λ for fermion atoms in a 2D optical lattice. λ is in units of t, and system parameters are the same as in Fig. 3.

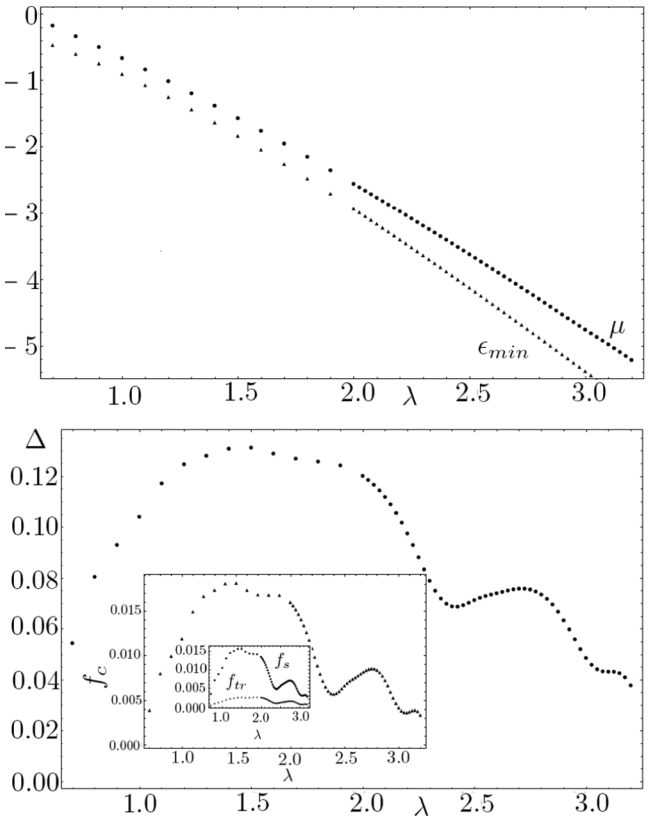

FIG. 9. Zero-temperature chemical potential, gap, and singlet f_s, triplet $f_{\rm tr}$, and full $f_c = f_s + f_{\rm tr}$ condensate fractions as a function of the Rashba SOC strength λ for fermion atoms in a 2D optical lattice without a Zeeman field. System parameters are $U = 2.5t$ and $f = 0.1$.

functional derivatives of the Fock Σ^F and the Hartree Σ^H self-energy $I = I_d + I_{\rm exc} = \delta\Sigma^F/\delta G + \delta\Sigma^H/\delta G$. Second, the collective excitations of the Hubbard model can be calculated as poles of the fermion two-particle Green's function, K, and as poles of the Green's function of the multicomponent boson field, D. Third, the action which describes the interactions in the Hubbard model is similar to the action $\psi^\dagger A\psi$ in quantum electrodynamics. For this reason we can utilize powerful field-theoretical methods, such as the method of Legendre transforms, to derive the Schwinger-Dyson (SD) equation of the boson Green's function $\widehat{D}$, the BS equation of the two-particle Green's function, and the corresponding equation for the vertex function.

Thus, in the aforementioned manner, the quartic terms are transformed into the quadratic form by inserting a four-component boson field $A_\alpha(z)$ which mediates the interaction of fermions $\widehat{\overline{\psi}}(y) = \widehat{\Psi}^\dagger(y)/\sqrt{2}$ and $\widehat{\psi}(x) = \widehat{\Psi}(x)/\sqrt{2}$ [$\alpha = 1,2,3,4$, $z = (\mathbf{r}_i, v)$], where

$$\widehat{\Psi}(x) = \begin{pmatrix} \psi_\uparrow(x) \\ \psi_\downarrow(x) \\ \psi_\uparrow^\dagger(x) \\ \psi_\downarrow^\dagger(x) \end{pmatrix},$$

$$\widehat{\Psi}^\dagger(y) = (\psi_\uparrow^\dagger(y),\ \psi_\downarrow^\dagger(y),\ \psi_\uparrow(y),\ \psi_\downarrow(y)).$$

The single-particle Green's function, introduced in the previous section, can be written as a tensor product between the two matrices $\widehat{\Psi}(x_1)$ and $\widehat{\Psi}^\dagger(y_2)$; i.e., $\widehat{G}(x_1; y_2) = -\langle \widehat{T}_u(\widehat{\Psi}(x_1) \otimes \widehat{\overline{\Psi}}(y_2))\rangle$. As in quantum electrodynamics, where the photons mediate the interaction of electric charges, we define an action of the form $S = S_0^{(F)} + S_0^{(B)} + S^{(F-B)}$, where $S_0^{(F)} = \widehat{\overline{\psi}}(y)\widehat{G}^{(0)-1}(y;x)\widehat{\psi}(x)$, $S_0^{(B)} = \frac{1}{2}A_\alpha(z)D_{\alpha\beta}^{(0)-1}(z,z')A_\beta(z')$, and $S^{(F-B)} = \widehat{\overline{\psi}}(y)\widehat{\Gamma}_\alpha^{(0)}(y,x \mid z)\widehat{\psi}(x)A_\alpha(z)$. The action $S_0^{(F)}$ describes the fermion part of the system. The generalized inverse Green's function of free fermions $\widehat{G}^{(0)-1}(y;x)$ is given by the following 4×4 matrix:

$$\widehat{G}^{(0)-1}(y;x) = \sum_{\mathbf{k},\omega_m} e^{[\imath\mathbf{k}\cdot(\mathbf{r}_i - \mathbf{r}_{i'}) - \omega_m(u-u')]}\widehat{G}^{(0)-1}(\mathbf{k}, \imath\omega_m).$$

In the case of the population-balanced Fermi gas with planar Rashba SOC and an out-of-plane Zeeman field, the noninteracting Green's function is

$$\widehat{G}^{(0)-1}(\mathbf{k}, \imath\omega_m) = \begin{pmatrix} g_{11}^{(0)-1} & 0 \\ 0 & g_{22}^{(0)-1} \end{pmatrix},$$

where

$$g_{11}^{(0)-1} = \begin{pmatrix} \imath\omega_m - \xi(\mathbf{k}) - h & -2\lambda(\sin k_y + \imath \sin k_x) \\ -2\lambda(\sin k_y - \imath \sin k_x) & \imath\omega_m - \xi(\mathbf{k}) + h \end{pmatrix},$$

$$g_{22}^{(0)-1} = \begin{pmatrix} \imath\omega_m + \xi(\mathbf{k}) + h & -2\lambda(\sin k_y - \imath \sin k_x) \\ -2\lambda(\sin k_y + \imath \sin k_x) & \imath\omega_m + \xi(\mathbf{k}) - h \end{pmatrix}.$$

The action $S_0^{(B)}$ describes the boson field, which mediates the fermion-fermion on-site interaction in the Hubbard Hamiltonian. The bare boson propagator $\widehat{D}^{(0)}$ is defined as

$$\widehat{D}^{(0)}(z,z') = \delta(v - v')U\delta j, j' \begin{pmatrix} 0 & 1 & 0 & 0 \\ 1 & 0 & 0 & 0 \\ 0 & 0 & 0 & 0 \\ 0 & 0 & 0 & 0 \end{pmatrix}.$$

The Fourier transform of the above boson propagator is given by

$$\widehat{D}^{(0)}(z,z') = \frac{1}{N}\sum_{\mathbf{k}}\sum_{\omega_p} e^{\{\imath[\mathbf{k}\cdot(\mathbf{r}_j - \mathbf{r}_{j'}) - \omega_p(v-v')]\}}\widehat{D}^{(0)}(\mathbf{k}),$$

$$\widehat{D}^{(0)}(\mathbf{k}) = \begin{pmatrix} 0 & U & 0 & 0 \\ U & 0 & 0 & 0 \\ 0 & 0 & 0 & 0 \\ 0 & 0 & 0 & 0 \end{pmatrix}.$$

Here the symbol $\sum_{\omega_p}$ is used to denote $\beta^{-1}\sum_p$ [for a boson field $\omega_p = (2\pi/\beta)p$, $p = 0, \pm 1, \pm 2, \ldots$].

The interaction between the fermion and the boson fields is described by the action $S^{(F-B)}$. The bare vertex $\widehat{\Gamma}_\alpha^{(0)}(y_1; x_2 \mid z) = \widehat{\Gamma}_\alpha^{(0)}(i_1, u_1; i_2, u_2 \mid j, v) = \delta(u_1 - u_2)\delta(u_1 - v)\delta_{i_1 i_2}\delta_{i_1 j}\widehat{\Gamma}^{(0)}(\alpha)$ is a 4×4 matrix, where

$$\widehat{\Gamma}^{(0)}(\alpha) = \tfrac{1}{2}(\gamma_0 + \alpha_z)\delta_{\alpha 1} + \tfrac{1}{2}(\gamma_0 - \alpha_z)\delta_{\alpha 2} + \tfrac{1}{2}(\alpha_x + \imath\alpha_y)\delta_{\alpha 3} + \tfrac{1}{2}(\alpha_x - \imath\alpha_y)\delta_{\alpha 4}. \quad (6)$$

The Dirac matrix γ_0 and the matrices $\widehat{\alpha}_i$ are defined such that when a four-dimensional space is used, the electron spin operators σ_i must be replaced with $\widehat{\alpha}_i\gamma_0$ [44]:

$$\gamma_0 = \begin{pmatrix} 1 & 0 & 0 & 0 \\ 0 & 1 & 0 & 0 \\ 0 & 0 & -1 & 0 \\ 0 & 0 & 0 & -1 \end{pmatrix},$$

$$\widehat{\alpha}_i = \begin{pmatrix} \sigma_i & 0 \\ 0 & \sigma_y\sigma_i\sigma_y \end{pmatrix}, \quad i = x,y,z.$$

The relationship between the Hubbard model and our model system can be demonstrated by applying the Hubbard-Stratonovich transformation for the fermion operators:

$$\int D\mu[A] \exp\left[\widehat{\overline{\psi}}(y)\widehat{\Gamma}^{(0)}_{\alpha}(y;x|z)\widehat{\psi}(x)A_\alpha(z)\right]$$
$$= \exp\left[-\tfrac{1}{2}\widehat{\overline{\psi}}(y)\widehat{\Gamma}^{(0)}_{\alpha}(y;x|z)\widehat{\psi}(x)D^{(0)}_{\alpha,\beta}(z,z')\widehat{\overline{\psi}}(y')\widehat{\Gamma}^{(0)}_{\beta}\right.$$
$$\left.\times(y';x'|z')\widehat{\psi}(x')\right]. \tag{7}$$

The functional measure $D\mu[A]$ is chosen to be

$$D\mu[A] = DAe^{-\frac{1}{2}A_\alpha(z)D^{(0)-1}_{\alpha,\beta}(z,z')A_\beta(z')}, \quad \int D\mu[A] = 1.$$

Next, we apply a functional integral technique to derive the BS equation for the poles [collective modes $\omega = \omega(\mathbf{Q})$] of the two-particle Green's function in the GRPA. By following the standard procedures in the functional integral formalism [45,46], it is possible to derive the SD equation $G^{-1} = G^{(0)-1} - \Sigma$ and the BS equation $[K^{(0)-1} - I]\Psi = 0$ for the poles of the single-particle Green's function G and the poles of the two-particle Green's function, respectively [47–49]. Here, $G^{(0)}$ is the free single-particle propagator, Σ is the fermion self-energy, I is the BS kernel, and the two-particle free propagator $K^{(0)} = GG$ is the product of two fully dressed single-particle Green's functions. The kernel of the BS equation is defined as the sum of the direct interaction $I_d = \delta\Sigma^F/\delta G$ and the exchange interaction $I_{\rm exc} = \delta\Sigma^H/\delta G$, where Σ^F and Σ^H are the Fock and the Hartree parts of the fermion self-energy Σ. Since the fermion self-energy depends on the two-particle Green's function, the positions of both poles must be obtained by resolving the SD and BS equations self-consistently.

In practice, the GRPA permits us to decouple the SD equations from the BS equation. According to this approximation, the single-particle excitations are calculated in the mean-field approximation, while the collective modes are obtained by solving the BS equation in which the single-particle Green's functions are determined in the Hartree-Fock approximation and the BS kernel takes into account contributions from both ladder diagrams (direct interaction) and bubble diagrams (exchange interaction). Explicitly, the single-particle mean-field Green's function is

$$\widehat{G}^{-1}_{\rm MF}(\mathbf{k},\imath\omega_m) = \begin{pmatrix} g^{(0)-1}_{11} & \imath\Delta\sigma_y \\ -\imath\Delta\sigma_y & g^{(0)-1}_{22} \end{pmatrix}. \tag{8}$$

In the GRPA the direct interaction in the BS kernel is calculated by a linearized Fock term and exact Hartree term:

$$\Sigma^F_0(i_1,u_1;i_2,u_2)_{n_1,n_2} = -U\delta_{i_1,i_2}\delta(u_1-u_2)\begin{pmatrix} 0 & G_{12} & 0 & -G_{14} \\ G_{21} & 0 & -G_{23} & 0 \\ 0 & G_{32} & 0 & G_{34} \\ -G_{41} & 0 & G_{43} & 0 \end{pmatrix},$$
$$\Sigma^H(i_1,u_1;i_2,u_2) = \frac{U}{2}\delta_{i_1,i_2}\delta(u_1-u_2)\begin{pmatrix} G_{22}-G_{44} & 0 & 0 & 0 \\ 0 & G_{11}-G_{33} & 0 & 0 \\ 0 & 0 & G_{44}-G_{22} & 0 \\ 0 & 0 & 0 & G_{33}-G_{11} \end{pmatrix}, \tag{9}$$

where $G_{i,j} \equiv G_{i,j}(1;2) = G_{i,j}(i_1,u_1;i_2,u_2)$. In the GRPA the BS equation for the 16 BS amplitudes $\Psi^{\mathbf{Q}}_{n_2,n_1}$, $\{n_1,n_2\} = \{1,2,3,4\}$, is

$$\Psi^{\mathbf{Q}}_{n_2n_1} = K^{(0)}\begin{pmatrix} n_1 & n_3 \\ n_2 & n_4 \end{pmatrix}|\omega(\mathbf{Q})\Bigg)\left[I_d\begin{pmatrix} n_3 & n_5 \\ n_4 & n_6 \end{pmatrix} + I_{\rm exc}\begin{pmatrix} n_3 & n_5 \\ n_4 & n_6 \end{pmatrix}\right]\Psi^{\mathbf{Q}}_{n_6,n_5},$$

where

$$I_d\begin{pmatrix} n_1 & n_3 \\ n_2 & n_4 \end{pmatrix} = -\Gamma^{(0)}_\alpha(n_1,n_3)D^{(0)}_{\alpha\beta}\Gamma^{(0)}_\beta(n_4,n_2),$$
$$I_{\rm exc}\begin{pmatrix} n_1 & n_3 \\ n_2 & n_4 \end{pmatrix} = \frac{1}{2}\Gamma^{(0)}_\alpha(n_1,n_2)D^{(0)}_{\alpha\beta}\Gamma^{(0)}_\beta(n_4,n_3)$$

are the direct and exchange interactions, respectively. The two-particle free propagator $K^{(0)}$ in the GRPA is defined as follows:

$$K^{(0)}\begin{pmatrix} n_1 & n_3 \\ n_2 & n_4 \end{pmatrix}|\omega(\mathbf{Q})\Bigg) \equiv Kn_1n_3n_4n_2$$
$$= \int\frac{d\Omega}{2\pi}\int\frac{d^d\mathbf{k}}{(2\pi)^d}G^{\rm MF}_{n_1n_3}(\mathbf{k}+\mathbf{Q},\Omega+\omega(\mathbf{Q}))G^{\rm MF}_{n_4n_2}(\mathbf{k},\Omega).$$

The above BS equation can be rewritten in matrix form as $[\widehat{I} + U\widehat{M}(\omega,\mathbf{Q})]\widehat{\Psi} = 0$, where $\widehat{I}$ is the unit matrix and the transposed matrix of $\widehat{\Psi}$ is given by

$$\widehat{\Psi}^T = \big(\Psi^{\mathbf{Q}}_{1,1}, \Psi^{\mathbf{Q}}_{1,2}, \Psi^{\mathbf{Q}}_{1,3}, \Psi^{\mathbf{Q}}_{1,4}, \Psi^{\mathbf{Q}}_{2,1}, \Psi^{\mathbf{Q}}_{2,2}, \Psi^{\mathbf{Q}}_{2,3}, \Psi^{\mathbf{Q}}_{2,4}, \times \Psi^{\mathbf{Q}}_{3,1}, \Psi^{\mathbf{Q}}_{3,2}, \Psi^{\mathbf{Q}}_{3,3}, \Psi^{\mathbf{Q}}_{3,4}, \Psi^{\mathbf{Q}}_{4,1}, \Psi^{\mathbf{Q}}_{4,2}, \Psi^{\mathbf{Q}}_{4,3}, \Psi^{\mathbf{Q}}_{4,4}\big).$$

The non-trivial solution of the BS equation requires that the 16×16 determinant $\det|\widehat{I} + U\widehat{M}(\omega,\mathbf{Q})| = 0$, and this condition provides the collective excitation spectrum $\omega(\mathbf{Q})$. By applying simple matrix algebra, the 16×16 determinant $\det|\widehat{I} + U\widehat{M}(\omega,\mathbf{Q})| = 0$ can be simplified to a 10×10 determinant. Thus, the collective excitation spectrum $\omega(\mathbf{Q})$ at a given momentum $\mathbf{Q}$ is defined by $Z(\omega,\mathbf{Q}) = 0$, where

$$Z(\omega,\mathbf{Q}) = \det\begin{vmatrix} G_{2\times2}(\omega,\mathbf{Q}) & D_{2\times8}(\omega,\mathbf{Q}) \\ D_{8\times2}(\omega,\mathbf{Q}) & C_{8\times8}(\omega,\mathbf{Q}) \end{vmatrix}. \tag{10}$$

Here $D_{2\times8}(\omega,\mathbf{Q}) = [D_{8\times2}(\omega,\mathbf{Q})]^T$, and the elements of the blocks $G_{2\times2}(\omega,\mathbf{Q})$, $B_{8\times2}(\omega,\mathbf{Q})$, and $C_{8\times8}(\omega,\mathbf{Q})$ are defined in Appendix B.

In the Gaussian approximation, the collective excitation spectrum $\omega_G(\mathbf{Q})$ is defined by the equation $G_G(\omega,\mathbf{Q}) = 0$, where

$$G_G(\omega,\mathbf{Q}) = \det|G_{2\times2}(\omega,\mathbf{Q})|. \tag{11}$$

In the BS approach, when all single-particle Green's functions are taken into account, the collective excitation spectrum $\omega_{\rm BS}(\mathbf{Q})$ is defined by the equation $G_{\rm BS}(\omega,\mathbf{Q}) = 0$, where

$$G_{\rm BS}(\omega,\mathbf{Q}) = \det\big|G_{2\times2}(\omega,\mathbf{Q}) - D_{2\times8}(\omega,\mathbf{Q})C^{-1}_{8\times8}(\omega,\mathbf{Q})D_{8\times2}(\omega,\mathbf{Q})\big|. \tag{12}$$

In Fig. 10, we have plotted the speed of sound along x-direction $[\mathbf{Q} = (Q_x,0)]$ as a function of the SOC strength, calculated within the Gaussian approximation and from the BS equation. Close to the point where the chemical potential becomes negative, the speed of sound has a local maximum. As can be seen, the Gaussian approximation overestimates the speed of sound, and the difference between the two approaches is about 15%. This can be related to the fact that the Gaussian approximation does not take into account the exchange interaction. The speed of sound exhibits different behavior compared to the continuum: in the 3D and 2D continua the slope of the Goldstone mode decreases as a function of the SOC strength [15], while in the lattice case the speed of sound increases monotonically with the SOC strength.

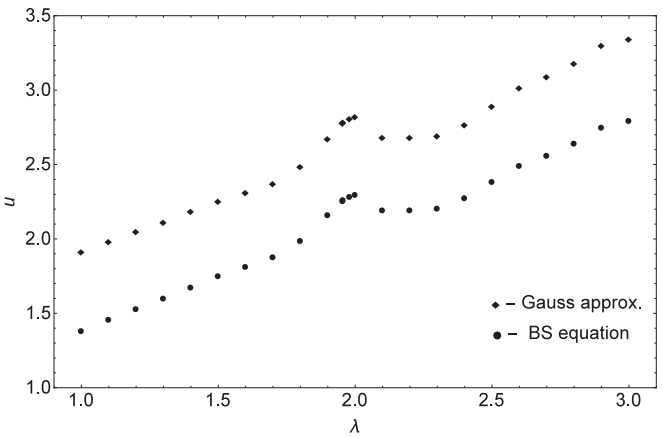

FIG. 10. The speeds of the sound u along the Q_x direction calculated in the Gaussian (circles) and in the Bethe-Salpeter (squares) approximations as functions of the Rashba SOC strength λ. The SOC strength is in units of t, while the speed of sound is in units of $ta/\hbar$. The system parameters are the same as in Fig. 3.

Next, we apply the BS formalism to derive an equation for the bound-state energy and show that it is equivalent to the bound-state equation in the Gaussian approximation when $\Delta = 0$. In both cases, we set $\mathbf{Q} = 0$, and the two-body problem follows from our many-body description by setting $\omega - \mu = E_B$. In this limit, the Gaussian block $G_{2\times2}$ assumes a diagonal form,

$$G_{2\times2}(\omega,\mathbf{Q}) = \begin{vmatrix} g_G(\omega,\mathbf{Q}) & 0 \\ 0 & g_G(-\omega,\mathbf{Q}) \end{vmatrix}, \tag{13}$$

where

$$g_G(\omega,\mathbf{Q}) = 1 + \frac{U}{2}[K_{1144}(\omega,\mathbf{Q}) + K_{2233}(\omega,\mathbf{Q}) - 2K_{1234}(\omega,\mathbf{Q})].$$

Thus, in the Gaussian approximation the determinant $\det|G_{2\times2}(\omega = E_B + \mu,\mathbf{Q} = 0)| = 0$ provides the bound-state equation at zero temperature, (1). The BS equation for the bound-state energy follows from (12); we can obtain the following BS equation for the bound-state energy $g_{\rm BS}(E_B + \mu,0) = 0$, where

$$g_{\rm BS}(\omega,\mathbf{Q}) = (1 + U[K_{1144}(\omega,\mathbf{Q}) - K_{2233}(\omega,\mathbf{Q})]) \times (1 + U[K_{1144}(\omega,\mathbf{Q}) + K_{2233}(\omega,\mathbf{Q})]). \tag{14}$$

As can be seen, if $\Delta = 0$, we have $K_{1144}(\omega,\mathbf{Q}) = K_{2233}(\omega,\mathbf{Q})$, and therefore, we reobtain the two-body bound-state equation, (1), in the Gaussian approximation.

We have numerically solved the bound-state equation, (1), for different strengths of SOC, assuming that the Zeeman field is $h = 0.4t$ and $U = 5t$, and plotted the results in Fig. 11. As in the continuum, an increase in the SOC strength λ leads to a deeper bound state which approaches $2\epsilon_{\rm min}$.

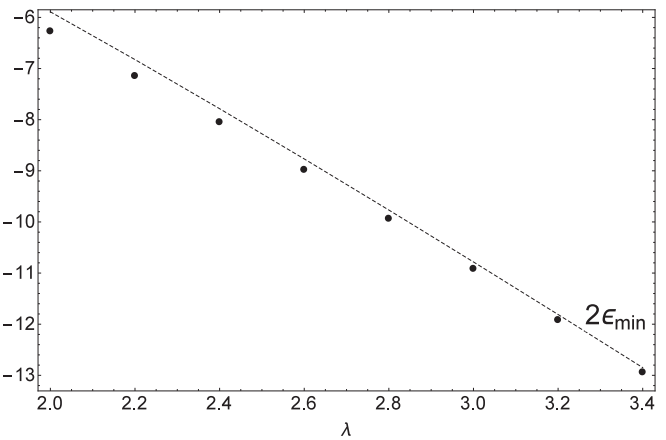

FIG. 11. The bound-state energy E_B as a function of the Rashba SOC strength λ at $U = 5t$ and $h = 0.4t$. The dashed line is twice the single-particle minimum energy $2\epsilon_{\rm min}$. The SOC strength and all energies are in units of t.

IV. SUMMARY

In summary, we have presented a comprehensive study of the single-particle and collective excitations of a Rashba spin-orbit-coupled atomic Fermi gas with attractive interaction, loaded in a 2D square optical lattice, in the presence of an effective out-of-plane Zeeman field. We calculated important and experimentally relevant physical quantities, such as the chemical potential, the pairing gap, the singlet and triplet pairing correlations, the singlet and triplet condensate fractions, and the speed of sound. All of these quantities are strongly modified compared to the Fermi gases in free space. In particular, we have found entirely different behavior (compared to the continuum) of the gap, the condensate fraction, and the speed of sound as functions of the SOC strength, whereas the mean-field quantities are similar to those in the non-Abelian SOC lattice case, even though that case did not have a Zeeman field. To the best of our knowledge, there is no other calculation of the speed of sound in a lattice case as a function of the SOC strength with which we can make comparisons. Finally, we have shown that our Bethe-Salpeter formalism is equivalent to the Gaussian approximation for $\Delta = 0$.

APPENDIX A: MEAN-FIELD SINGLE-PARTICLE GREEN's FUNCTION

Under the Nambu spinor basis $\widehat{\Psi} = (\psi_{\mathbf{k},\uparrow}, \psi_{\mathbf{k},\downarrow}, \psi^{\dagger}_{-\mathbf{k},\uparrow}, \psi^{\dagger}_{-\mathbf{k},\downarrow})^T$ for the field operators, the Fourier transform of the single-particle mean-field Green's function $\hat{G}^{\mathrm{MF}}(x_1, y_2)$ is

$$\widehat{G}^{\mathrm{MF}}(\mathbf{k},\imath\omega_m) = \begin{pmatrix} \hat{g}(\mathbf{k},\imath\omega_m) & \hat{f}(\mathbf{k},\imath\omega_m) \\ [\hat{f}(\mathbf{k},-\imath\omega_m)]^{\dagger} & -[\hat{g}(-\mathbf{k},-\imath\omega_m)]^T \end{pmatrix},$$

where for fermion fields $\omega_m = (2\pi/\beta)(m + 1/2)$, $m = 0, \pm 1, \pm 2, \ldots$, and

$$\hat{g}(\mathbf{k},\imath\omega_m) = \begin{pmatrix} G^{\mathrm{MF}}_{11}(\mathbf{k},\imath\omega_m) & G^{\mathrm{MF}}_{12}(\mathbf{k},\imath\omega_m) \\ G^{\mathrm{MF}}_{21}(\mathbf{k},\imath\omega_m) & G^{\mathrm{MF}}_{22}(\mathbf{k},\imath\omega_m) \end{pmatrix},$$

$$\hat{f}(\mathbf{k},\imath\omega_m) = \begin{pmatrix} G^{\mathrm{MF}}_{13}(\mathbf{k},\imath\omega_m) & G^{\mathrm{MF}}_{14}(\mathbf{k},\imath\omega_m) \\ G^{\mathrm{MF}}_{23}(\mathbf{k},\imath\omega_m) & G^{\mathrm{MF}}_{24}(\mathbf{k},\imath\omega_m) \end{pmatrix}.$$

The matrix elements of $\hat{g}(\mathbf{k},\imath\omega_m)$ and $\hat{f}(\mathbf{k},\imath\omega_m)$ are given by

$$G^{\mathrm{MF}}_{ij}(\mathbf{k},\imath\omega_m) = \frac{A_{ij}(\mathbf{k},\omega_1,\omega_2)}{\imath\omega_m - \omega_1(\mathbf{k})} + \frac{B_{ij}(\mathbf{k},\omega_1,\omega_2)}{\imath\omega_m + \omega_1(\mathbf{k})} + \frac{A_{ij}(\mathbf{k},\omega_2,\omega_1)}{\imath\omega_m - \omega_2(\mathbf{k})} + \frac{B_{ij}(\mathbf{k},\omega_2,\omega_1)}{\imath\omega_m + \omega_2(\mathbf{k})}.$$

The mean-field single-particle excitations are defined by the four poles $\pm\omega_1(\mathbf{k})$ and $\pm\omega_2(\mathbf{k})$, where

$$\omega_1(\mathbf{k}) = [S(\mathbf{k}) + \Delta^2 + h^2 + \xi^2(\mathbf{k}) - 2\sqrt{h^2\Delta^2 + \xi^2(\mathbf{k})[h^2 + S(\mathbf{k})]}]^{1/2},$$

$$\omega_2(\mathbf{k}) = [S(\mathbf{k}) + \Delta^2 + h^2 + \xi^2(\mathbf{k}) + 2\sqrt{h^2\Delta^2 + \xi^2(\mathbf{k})[h^2 + S(\mathbf{k})]}]^{1/2}.$$

Here, Δ is the mean-field gap, $\xi(\mathbf{k}) = 2(1 - \cos k_x) + 2(1 - \cos k_y) - \mu$ is the tight-binding energy, and $S(\mathbf{k}) = |J(\mathbf{k})|^2$, such that $J(\mathbf{k}) = 2\lambda[\sin(k_y) + \imath \sin(k_x)]$, is the Rashba interaction. The explicit expressions of the elements of the $\hat{g}(\mathbf{k},\imath\omega_m)$ and $\hat{f}(\mathbf{k},\imath\omega_m)$ are as follows [the ω dependence of $M(\omega_1,\omega_2)$, $A_{ij}(\omega_1,\omega_2)$, and $B_{ij}(\omega_1,\omega_2)$, as well as the $\mathbf{k}$ dependence of $S(\mathbf{k})$, $J(\mathbf{k})$, $\xi(\mathbf{k})$, and $\omega_{1,2}(\mathbf{k})$, is understood):

$$M = 2\left(\omega_1^2 - \omega_2^2\right)\omega_1;$$

$$MA_{11} = -(h-\xi)(h^2 - \Delta^2 + S - \xi^2) - [\Delta^2 + S + (h-\xi)^2]\omega_1 + (h+\xi)\omega_1^2 + \omega_1^3;$$

$$MB_{11} = (h-\xi)(h^2 - \Delta^2 + S - \xi^2) - [\Delta^2 + S + (h-\xi)^2]\omega_1 - (h+\xi)\omega_1^2 + \omega_1^3;$$

$$MA_{22} = (h+\xi)(h^2 - \Delta^2 + S - \xi^2) - [\Delta^2 + S + (h+\xi)^2]\omega_1 + (-h+\xi)\omega_1^2 + \omega_1^3;$$

$$MB_{22} = -(h+\xi)(h^2 - \Delta^2 + S - \xi^2) - [\Delta^2 + S + (h+\xi)^2]\omega_1 + (h-\xi)\omega_1^2 + \omega_1^3;$$

$$MA_{12} = -J[h^2 + S + (\Delta - \xi - \omega_1)(\Delta + \xi + \omega_1)];$$

$$MB_{12} = J[h^2 + S + (\Delta + \xi - \omega_1)(\Delta - \xi - \omega_1)]; \quad MA_{21} = -J^*[h^2 + S + (\Delta - \xi - \omega_1)(\Delta + \xi + \omega_1)];$$

$$MB_{21} = J^*[h^2 + S + (\Delta + \xi - \omega_1)(\Delta - \xi + \omega_1)]; \quad MA_{13} = 2J\Delta(\xi - h); \quad MB_{13} = 2J\Delta(h - \xi);$$

$$MA_{24} = -2J^*\Delta(\xi + h); \quad MB_{24} = 2J^*\Delta(\xi + h); \quad MA_{14} = \Delta[S + \Delta^2 + \xi^2 - (h + \omega_1)^2];$$

$$MB_{14} = -\Delta[S + \Delta^2 + \xi^2 - (h - \omega_1)^2]; \quad MA_{23} = -\Delta[S + \Delta^2 + \xi^2 - (h - \omega_1)^2];$$

$$MB_{23} = \Delta[S + \Delta^2 + \xi^2 - (h + \omega_1)^2].$$

In the system under consideration, the number of particles is fixed, so the suitable thermodynamic potential is the Helmholtz free energy, given by

$$F(\Delta, f) = \frac{\Delta^2}{U} + \frac{1}{N}\sum_{\mathbf{k}}\left[\xi(\mathbf{k}) - \frac{1}{2}[\omega_1(\mathbf{k}) + \omega_2(\mathbf{k})] - \frac{1}{\beta}\{\ln(1 + e^{-\beta\omega_1(\mathbf{k})}) + \ln(1 + e^{-\beta\omega_2(\mathbf{k})})\}\right] + f\mu.$$

By minimizing the Helmholtz free energy with respect to the chemical potentials μ and the gap Δ, we obtain a set of two equations, namely, the number and gap equations:

$$\begin{aligned} f &= 1 - \frac{1}{N}\sum_{\mathbf{k}}\left[\frac{1}{2} - f_F(\omega_1(\mathbf{k}))\right]\frac{\xi(\mathbf{k})}{\omega_1(\mathbf{k})}\left(1 + \frac{S(\mathbf{k}) + h^2}{\sqrt{h^2\Delta^2 + \xi^2(\mathbf{k})[h^2 + S(\mathbf{k})]}}\right) \\ &\quad - \frac{1}{N}\sum_{\mathbf{k}}\left[\frac{1}{2} - f_F(\omega_2(\mathbf{k}))\right]\frac{\xi(\mathbf{k})}{\omega_2(\mathbf{k})}\left(1 - \frac{S(\mathbf{k}) + h^2}{\sqrt{h^2\Delta^2 + \xi^2(\mathbf{k})[h^2 + S(\mathbf{k})]}}\right), \\ 1 &= \frac{U}{N}\sum_{\mathbf{k}}\left[\frac{1}{2} - f_F(\omega_1(\mathbf{k}))\right]\frac{1}{2\omega_1(\mathbf{k})}\left(1 + \frac{h^2}{\sqrt{h^2\Delta^2 + \xi^2(\mathbf{k})[h^2 + S(\mathbf{k})]}}\right) \\ &\quad + \frac{1}{N}\sum_{\mathbf{k}}\left[\frac{1}{2} - f_F(\omega_2(\mathbf{k}))\right]\frac{1}{2\omega_2(\mathbf{k})}\left(1 - \frac{h^2}{\sqrt{h^2\Delta^2 + \xi^2(\mathbf{k})[h^2 + S(\mathbf{k})]}}\right). \end{aligned}$$

Here $f_F(z) = [\exp(\beta z) + 1]^{-1}$ is the Fermi distribution function. Using the corresponding matrix elements of the mean-field single-particle Green's function, we can evaluate the momentum distribution for the two spin components, $n_\uparrow(\mathbf{k}) = \langle\psi^\dagger_{\mathbf{k}\uparrow}\psi_{\mathbf{k}\uparrow}\rangle$ and $n_\downarrow(\mathbf{k}) = \langle\psi^\dagger_{\mathbf{k}\downarrow}\psi_{\mathbf{k}\downarrow}\rangle$:

$$\begin{aligned} n_\uparrow(\mathbf{k}) &= 1/2 - [1/2 - f_F(\omega_1(\mathbf{k}))]\frac{\xi(\mathbf{k})}{2\omega_1(\mathbf{k})}\left[1 - \frac{h^2 + S(\mathbf{k})}{\sqrt{S(\mathbf{k})\xi^2(\mathbf{k}) + h^2[\Delta^2 + \xi^2(\mathbf{k})]}}\right] \\ &\quad - [1/2 - f_F(\omega_2(\mathbf{k}))]\frac{\xi(\mathbf{k})}{2\omega_2(\mathbf{k})}\left[1 + \frac{h^2 + S(\mathbf{k})}{\sqrt{S(\mathbf{k})\xi^2(\mathbf{k}) + h^2\left[\Delta^2 + \xi^2(\mathbf{k})\right]}}\right] \\ &\quad - [1/2 - f_F(\omega_1(\mathbf{k}))]\frac{h}{2\omega_1(\mathbf{k})}\left[1 - \frac{\Delta^2 + \xi^2(\mathbf{k})}{\sqrt{S(\mathbf{k})\xi^2(\mathbf{k}) + h^2[\Delta^2 + \xi^2(\mathbf{k})]}}\right] \\ &\quad - [1/2 - f_F(\omega_2(\mathbf{k}))]\frac{h}{2\omega_2(\mathbf{k})}\left[1 + \frac{\Delta^2 + \xi^2(\mathbf{k})}{\sqrt{S(\mathbf{k})\xi^2(\mathbf{k}) + h^2[\Delta^2 + \xi^2(\mathbf{k})]}}\right]; \\ n_\downarrow(\mathbf{k}) &= 1/2 - [1/2 - f_F(\omega_1(\mathbf{k}))]\frac{\xi(\mathbf{k})}{2\omega_1(\mathbf{k})}\left[1 - \frac{h^2 + S(\mathbf{k})}{\sqrt{S(\mathbf{k})\xi^2(\mathbf{k}) + h^2[\Delta^2 + \xi^2(\mathbf{k})]}}\right] \\ &\quad - [1/2 - f_F(\omega_2(\mathbf{k}))]\frac{\xi(\mathbf{k})}{2\omega_2(\mathbf{k})}\left[1 + \frac{h^2 + S(\mathbf{k})}{\sqrt{S(\mathbf{k})\xi^2(\mathbf{k}) + h^2[\Delta^2 + \xi^2(\mathbf{k})]}}\right] \\ &\quad + [1/2 - f_F(\omega_1(\mathbf{k}))]\frac{h}{2\omega_1(\mathbf{k})}\left[1 - \frac{\Delta^2 + \xi^2(\mathbf{k})}{\sqrt{S(\mathbf{k})\xi^2(\mathbf{k}) + h^2[\Delta^2 + \xi^2(\mathbf{k})]}}\right] \\ &\quad + [1/2 - f_F(\omega_2(\mathbf{k}))]\frac{h}{2\omega_2(\mathbf{k})}\left[1 + \frac{\Delta^2 + \xi^2(\mathbf{k})}{\sqrt{S(\mathbf{k})\xi^2(\mathbf{k}) + h^2[\Delta^2 + \xi^2(\mathbf{k})]}}\right]. \end{aligned}$$

Another interesting feature of the SOC is that the pairing field contains both a singlet and a triplet component. The singlet, $\Phi_{\downarrow\uparrow}(\mathbf{k}) = -\Phi_{\uparrow\downarrow}(\mathbf{k}) = \langle\psi_{\mathbf{k}\downarrow}\psi_{-\mathbf{k}\uparrow}\rangle$, and triplet, $\Phi_{\uparrow\uparrow}(\mathbf{k}) = \langle\psi_{\mathbf{k}\uparrow}\psi_{-\mathbf{k}\uparrow}\rangle$ and $\Phi_{\downarrow\downarrow}(\mathbf{k}) = \langle\psi_{\mathbf{k}\downarrow}\psi_{-\mathbf{k}\downarrow}\rangle$, amplitudes, obtained by means of the Green's function elements, G_{23}, G_{13}, and G_{24}, are

$$\begin{aligned} \Phi_{\downarrow\uparrow}(\mathbf{k}) &= \frac{\Delta[1/2 - f_F(\omega_2(\mathbf{k}))]}{2\omega_2(\mathbf{k})}\left[1 + \frac{h^2}{\sqrt{S(\mathbf{k})\xi^2(\mathbf{k}) + h^2[\Delta^2 + \xi^2(\mathbf{k})]}}\right] \\ &\quad + \frac{\Delta[1/2 - f_F(\omega_1(\mathbf{k}))]}{2\omega_1(\mathbf{k})}\left[1 - \frac{h^2}{\sqrt{S(\mathbf{k})\xi^2(\mathbf{k}) + h^2[\Delta^2 + \xi^2(\mathbf{k})]}}\right]; \\ \Phi_{\uparrow\uparrow}(\mathbf{k}) &= \frac{\Delta J(\mathbf{k})[h - \xi(\mathbf{k})]}{2\sqrt{S(\mathbf{k})\xi^2(\mathbf{k}) + h^2[\Delta^2 + \xi^2(\mathbf{k})]}}\left[\frac{1/2 - f_F(\omega_2(\mathbf{k}))}{\omega_2(\mathbf{k})} - \frac{1/2 - f_F(\omega_1(\mathbf{k}))}{\omega_1(\mathbf{k})}\right]; \end{aligned}$$

$$\Phi_{\downarrow\downarrow}(\mathbf{k}) = \frac{\Delta J^*(\mathbf{k})[h+\xi(\mathbf{k})]}{2\sqrt{S(\mathbf{k})\xi^2(\mathbf{k})+h^2[\Delta^2+\xi^2(\mathbf{k})]}}\left[\frac{1/2-f_F(\omega_2(\mathbf{k}))}{\omega_2(\mathbf{k})}-\frac{1/2-f_F(\omega_1(\mathbf{k}))}{\omega_1(\mathbf{k})}\right].$$

With the help of the pairing amplitudes, one can calculate the condensate fraction $f_c = f_s + f_{\rm tr}$, where f_s and $f_{\rm tr}$ are the singlet and triplet contributions, respectively. At zero temperature, we obtain

$$\begin{aligned} f_s &= \frac{2}{N}\sum_{\mathbf{k}}|\Phi_{\downarrow\uparrow}(\mathbf{k})|^2 \\ &= \frac{\Delta^2}{8N}\sum_{\mathbf{k}}\left[\frac{1}{\omega_2(\mathbf{k})}\left(1+\frac{h^2}{\sqrt{S(\mathbf{k})\xi^2(\mathbf{k})+h^2[\Delta^2+\xi^2(\mathbf{k})]}}\right)+\frac{1}{\omega_1(\mathbf{k})}\left(1-\frac{h^2}{\sqrt{S(\mathbf{k})\xi^2(\mathbf{k})+h^2[\Delta^2+\xi^2(\mathbf{k})]}}\right)\right]^2, \\ f_{\rm tr} &= \frac{1}{N}\sum_{\mathbf{k}}(|\Phi_{\uparrow\uparrow}(\mathbf{k})|^2+|\Phi_{\downarrow\downarrow}(\mathbf{k})|^2) = \frac{\Delta^2}{8N}\sum_{\mathbf{k}}\frac{S(\mathbf{k})[h^2+\xi^2(\mathbf{k})]}{S(\mathbf{k})\xi^2(\mathbf{k})+h^2[\Delta^2+\xi^2(\mathbf{k})]}\left[\frac{1}{\omega_2(\mathbf{k})}-\frac{1}{\omega_1(\mathbf{k})}\right]^2. \end{aligned}$$

APPENDIX B: BETHE-SALPETER SECULAR DETERMINANT

The elements of the $G_{2\times2}(\omega,\mathbf{Q})$ and the $D_{8\times2}(\omega,\mathbf{Q})$ blocks are as follows:

$$\begin{aligned} G_{11} &= 1+\frac{U}{2}(K2233-K1234-K2143+K1144), \\ G_{12} &= \frac{U}{2}(K1414-K2413-K1324+K2323), \\ G_{21} &= \frac{U}{2}(K4141-K4231-K3142+K3232), \\ G_{22} &= 1+\frac{U}{2}(K3322-K3412-K4321+K4411). \end{aligned}$$

Note that $K_{2143}(\omega,\mathbf{Q})$ [$K_{3412}(\omega,\mathbf{Q})$] is a complex conjugate of $K_{1234}(\omega,\mathbf{Q})$ [$K_{4321}(\omega,\mathbf{Q})$]:

$$\begin{aligned} D_{11} &= -\frac{1}{2}-\frac{U}{2}(K3322-K3412), \quad D_{12} = \frac{U}{2}(K2323-K1324), \\ D_{21} &= \frac{U}{2}(K1414-K1324), \quad D_{22} = -\frac{1}{2}-\frac{U}{2}(K1144-K1234), \\ D_{31} &= \frac{U}{2}(K2322-K2412-K3442+K4414), \\ D_{32} &= \frac{U}{2}(K1224-K1444-K2223+K2443), \\ D_{41} &= \frac{U}{2}(K1321-K1411-K3323+K3414), \\ D_{42} &= \frac{U}{2}(K1114-K1231-K1334+K2333), \\ D_{51} &= \frac{U}{2}(K2411-K2321), \quad D_{52} = \frac{U}{2}(K1214-K2213). \\ D_{61} &= \frac{U}{2}(K1412-K1322), \quad D_{62} = \frac{U}{2}(K1124+K1232), \\ D_{71} &= \frac{U}{2}(K3432+K4413), \quad D_{72} = \frac{U}{2}(K1434-K2433) \\ D_{81} &= \frac{U}{2}(K3414-K3324), \quad D_{82} = \frac{U}{2}(K1344-K2343). \end{aligned}$$

The 8×8 block $C_{8\times8}(\omega,\mathbf{Q})$ is a symmetric block:

$$\begin{aligned} C_{11} &= \frac{1}{2}+\frac{U}{2}K3322, \quad C_{12} = \frac{U}{2}K1324, \quad C_{13} = \frac{U}{2}(K3442-K2322), \\ C_{14} &= \frac{U}{2}(K3323-K1321), \quad C_{15} = \frac{U}{2}K2321, \quad C_{16} = \frac{U}{2}K1322 \end{aligned}$$

$$C_{17} = -\frac{U}{2}K3432, \quad C_{18} = \frac{U}{2}K3324, \quad C_{22} = \frac{1}{2} + \frac{U}{2}K1144,$$
$$C_{23} = \frac{U}{2}(K1444 - K1224), \quad C_{24} = \frac{U}{2}(K1334 - K1114),$$
$$C_{25} = -\frac{U}{2}K1214, \quad C_{26} = -\frac{U}{2}K1124, \quad C_{27} = -\frac{U}{2}K1434,$$
$$C_{28} = -\frac{U}{2}K1344, \quad C_{33} = \frac{U}{2}(K2222 - K2442 - K4224 + K4444),$$
$$C_{34} = 1 + \frac{U}{2}(K1221 - K1441 - K2332 + K3443),$$
$$C_{35} = \frac{U}{2}(K2212 + K2441), \quad C_{36} = \frac{U}{2}(K1442 - K1222),$$
$$C_{37} = \frac{U}{2}(K2432 - K4434), \quad C_{38} = \frac{U}{2}(K2342 + K3444),$$
$$C_{44} = \frac{U}{2}(K1111 - K1331 - K3113 + K3333), \quad C_{45} = \frac{U}{2}(K1211 + K2331),$$
$$C_{46} = \frac{U}{2}(K1332 - K1112), \quad C_{47} = \frac{U}{2}(K1431 - K3433),$$
$$C_{48} = \frac{U}{2}(K1341 + K3334), \quad C_{55} = \frac{1}{2} - \frac{U}{2}K2211, \quad C_{56} = -\frac{U}{2}K1212,$$
$$C_{57} = -\frac{U}{2}K2431, \quad C_{58} = -\frac{U}{2}K2341, \quad C_{66} = \frac{1}{2} - \frac{U}{2}K1122,$$
$$C_{67} = -\frac{U}{2}K1432, \quad C_{68} = -\frac{U}{2}K1342, \quad C_{77} = \frac{1}{2} - \frac{U}{2}K4433,$$
$$C_{78} = -\frac{U}{2}K3434, \quad C_{88} = \frac{1}{2} - \frac{U}{2}K3344.$$

[1] Y.-J. Lin, R. L. Compton, A. R. Perry, W. D. Phillips, J. V. Porto, and I. B. Spielman, Phys. Rev. Lett. **102**, 130401 (2009).

[2] Y.-J. Lin, R. L. Compton, K. Jiménez-García, J. V. Porto, and I. B. Spielman, Nature **462**, 628 (2009).

[3] Y.-J. Lin, K. Jimenez-Garcia, and I. B. Spielman, Nature **471**, 83 (2011).

[4] M. Sato, Y. Takahashi, and S. FujimotoPhys. Rev. Lett. **103**, 020401 (2009).

[5] J. P. Vyasanakere and V. B. Shenoy, Phys. Rev. B **83**, 094515 (2011); Phys. Rev. A **86**, 053617 (2012).

[6] J. P. Vyasanakere, S. Zhang, and V. B. Shenoy, Phys. Rev. B **84**, 014512 (2011).

[7] L. Jiang, X.-J. Liu, H. Hu, and H. Pu, Phys. Rev. A **84**, 063618 (2011).

[8] L. Dell'Anna, G. Mazzarella, and L. Salasnich, Phys. Rev. A **84**, 033633 (2011).

[9] M. Gong, S. Tewari, and C. Zhang, Phys. Rev. Lett. **107**, 195303 (2011).

[10] H. Hu, L. Jiang, X.-J. Liu, and H. Pu, Phys. Rev. Lett. **107**, 195304 (2011).

[11] Z.-Q. Yu and H. Zhai, Phys. Rev. Lett. **107**, 195305 (2011).

[12] M. Iskin and A. L. Subasi, Phys. Rev. Lett. **107**, 050402 (2011).

[13] W. Yi and G.-C. Guo, Phys. Rev. A **84**, 031608(R) (2011).

[14] K. Zhou and Z. Zhang, Phys. Rev. Lett. **108**, 025301 (2012).

[15] L. He and X. G. Huang, Phys. Rev. Lett. **108**, 145302 (2012); Phys. Rev. B **86**, 014511 (2012); Ann. Phys. **337**, 163 (2013).

[16] L. Han and C. A. R. Sá de Melo, Phys. Rev. A **85**, 011606(R) (2012).

[17] H. Hu and X.-J. Liu, Phys. Rev. A **85**, 013619 (2012).

[18] M. Gong, G. Chen, S. Jia, and C. Zhang, Phys. Rev. Lett. **109**, 105302 (2012).

[19] G. Chen, M. Gong, and C. Zhang, Phys. Rev. A **85**, 013601 (2012).

[20] F. Wu, G.-C. Guo, W. Zhang, and W. Yi, Phys. Rev. Lett. **110**, 110401 (2013).

[21] J. Zhang, H. Hu, X.-J. Liu, and H. Pu, Annu. Rev. Cold At. Mol. **2**, 81 (2014).

[22] J. Devreese, J. Tempere, and C. A. R. Sa de Melo, Phys. Rev. Lett. **113**, 165304 (2014).

[23] C. Zhang, S. Tewari, R. M. Lutchyn, and S. Das Sarma, Phys. Rev. Lett. **101**, 160401 (2008).

[24] J. D. Sau, S. Tewari, R. M. Lutchyn, T. D. Stanescu, and S. Das Sarma, Phys. Rev. B **82**, 214509 (2010).

[25] I. I. Satija, D. C. Dakin, J. Y. Vaishnav, and C. W. Clark, Phys. Rev. A **77**, 043410 (2008).

[26] N. Goldman, A. Kubasiak, A. Bermudez, P. Gaspard, M. Lewenstein, and M. A. Martin-Delgado, Phys. Rev. Lett. **103**, 035301 (2009).

[27] N. Goldman, A. Kubasiak, P. Gaspard, and M. Lewenstein, Phys. Rev. A **79**, 023624 (2009).
[28] A. Kubasiak, P. Massignan, and M. Lewenstein, Europhys. Lett. **92**, 46004 (2010).
[29] L. Wang and L. Fu, Phys. Rev. A **87**, 053612 (2013).
[30] M. Iskin, Phys. Rev. A **88**, 013631 (2013).
[31] M. Burrello, I. C. Fulga, E. Alba, L. Lepori, and A. Trombettoni, Phys. Rev. A **88**, 053619 (2013).
[32] Q. Sun, G.-B. Zhu, W.-M. Liu, and A.-C. Ji, Phys. Rev. A **88**, 063637 (2013).
[33] Y. Zhang and C. Zhang, Phys. Rev. A **87**, 023611 (2013).
[34] F. Lin, C. Zhang, and V. W. Scarola, Phys. Rev. Lett. **112**, 110404 (2014).
[35] D. Toniolo and J. Linder, Phys. Rev. A **89**, 061605(R) (2014).
[36] C. Qu, M. Gong, and C. Zhang, Phys. Rev. A **89**, 053618 (2014).
[37] Y. Xu, C. Qu, M. Gong, and C. Zhang, Phys. Rev. A **89**, 013607 (2014).
[38] H. Zhai, Rep. Prog. Phys. **78**, 026001 (2015).
[39] H.-K. Tang, X. Yang, J. Sun, and H.-Q. Lin, Europhys. Lett. **107**, 40003 (2014).
[40] M. Iskin, Phys. Rev. A **93**, 013608 (2016).
[41] R. Combescot, M. Yu. Kagan, and S. Stringari, Phys. Rev. A **74**, 042717 (2006).
[42] G. E. Astrakharchik, J. Boronat, J. Casulleras, and S. Giorgini, Phys. Rev. Lett. **93**, 200404 (2004).
[43] G. Bertaina and S. Giorgini, Phys. Rev. Lett. **106**, 110403 (2011).
[44] K. Maki, in *Superconductivity*, edited by R. D. Parks (Marcel Dekker, New York, 1969), p. 1035.
[45] Z. Koinov, Sh. Pahl, and R. Mendoza, in *Horizons in World Physics*, Vol. 285 (Nova Science, Hauppauge, NY, 2015), Chap. 1.
[46] Z. Koinov and R. Mendoza, J. Low Temp. Phys. **184**, 1042 (2016).
[47] F. J. Dyson, Phys. Rev. **75**, 1736 (1949).
[48] J. Schwinger, Phys. Rev. **82**, 914 (1951).
[49] H. A. Bethe and E. E. Salpeter, Phys. Rev. **82**, 309 (1951); **84**, 1232 (1951).